© 2022. Published by The Company of Biologists Ltd | Development (2022) 149, dev199997. doi:10.1242/dev.199997

RESEARCH ARTICLE

Aster repulsion drives short-ranged ordering in the *Drosophila* syncytial blastoderm

Jorge de-Carvalho[1], Sham Tlili[2,*], Lars Hufnagel[3], Timothy E. Saunders[2,4,5,6,‡] and Ivo A. Telley[1,‡]

ABSTRACT

Biological systems are highly complex, yet notably ordered structures can emerge. During syncytial stage development of the *Drosophila melanogaster* embryo, nuclei synchronously divide for nine cycles within a single cell, after which most of the nuclei reach the cell cortex. The arrival of nuclei at the cortex occurs with remarkable positional order, which is important for subsequent cellularisation and morphological transformations. Yet, the mechanical principles underlying this lattice-like positional order of nuclei remain untested. Here, using quantification of nuclei position and division orientation together with embryo explants, we show that short-ranged repulsive interactions between microtubule asters ensure the regular distribution and maintenance of nuclear positions in the embryo. Such ordered nuclear positioning still occurs with the loss of actin caps and even the loss of the nuclei themselves; the asters can self-organise with similar distribution to nuclei in the wild-type embryo. The explant assay enabled us to deduce the nature of the mechanical interaction between pairs of nuclei. We used this to predict how the nuclear division axis orientation changes upon nucleus removal from the embryo cortex, which we confirmed *in vivo* with laser ablation. Overall, we show that short-ranged microtubule-mediated repulsive interactions between asters are important for ordering in the early *Drosophila* embryo and minimising positional irregularity.

KEY WORDS: Centrosome, Cytoskeleton, Force chains, Packing, *Ex vivo*, Microtubules, Syncytium, *Drosophila*

INTRODUCTION

Proliferation of the genome is a cornerstone of early development in all animals, generally achieved by rapid mitotic divisions. Almost all insects first segregate genome copies into hundreds of nuclei (in a syncytium) and only at a specific nuclear density transform the single cell into a tissue (Lecuit and Wieschaus, 2000). The distribution and separation of nuclei in syncytial embryos display surprising positional uniformity (Deneke et al., 2016; Kanesaki et al., 2011; Perondini et al., 1986; Sommer and Tautz, 1991). This uniformity is likely required for precise gene patterning and fate determination (Petkova et al., 2019). In *Drosophila melanogaster*, early nuclear divisions are meta-synchronous, whereby nuclei gradually fill the inner cellular space until, nine division cycles, or ∼80 min post-fertilisation, 300-400 of them arrive at the cell cortex (Foe and Alberts, 1983). The nuclei are subsequently embedded near the cortex of the ellipsoidal embryo, where they undergo four more rounds of division to generate ∼6000 nuclei (Krzic et al., 2012) before cellularisation. The spatiotemporal synchronisation of nuclear divisions is governed by a reaction-diffusion process of cell-cycle determinants emerging from nuclei (Deneke et al., 2016), and nuclear positioning is crucial for the synchronisation (Deneke et al., 2019).

How a syncytial embryo controls internuclear distance so robustly has been a decades-long topic of debate (von Dassow and Schubiger, 1994; Deneke et al., 2019; Dutta et al., 2019; Kaiser et al., 2018; Lv et al., 2020; Postner et al., 1992; Valdés-pérez and Minden, 1995). The microtubule dynamics are crucial for nuclear migration to the cortex at nuclear cycle (n.c.) 9 and for their regular distribution upon arrival (Baker et al., 1993; Foe and Alberts, 1983; Hatanaka and Okada, 1991; Zalokar and Erk, 1976). However, the requirement of microtubules for nuclear transport does not explain the emergence of a uniform nuclear distribution at the cortex. Nuclei could be embedded in a regular matrix that either pulls or pushes them apart, leading to precise internuclear distances. For example, in the syncytial embryo of the cricket, a pulling mechanism has been proposed to distribute nuclei towards the embryo periphery (Donoughe et al., 2021 preprint). Recent work has shown that interaction between spindles and F-actin is essential for the pseudo-synchronised mitotic divisions (Lv et al., 2020), but the role of such interactions in ensuring uniform nuclear distribution is unclear. It has also been proposed that microtubule motor-based repulsion of nuclei can drive nuclear patterning (Baker et al., 1993; Lv et al., 2018), but this remains untested *in vivo*. In summary, despite extensive study, the mechanical aspects of robust nuclear positioning in the syncytium remain unresolved.

In interphase of the cell cycle, microtubules are organised in radial arrays called ‘asters’, which grow from and are organised by the centrosome (Callaini and Riparbelli, 1990). The centrosome acts as the main microtubule organising centre (MTOC) and promotes polymerisation and focusing of microtubules (Paz and Lüders, 2018). Two asters are linked to each nucleus, being functional elements of the bipolar spindle during mitosis. In a cell-cycle mutant (*gnu*), asters dissociate from the nucleus, grow large and distribute around the single giant nucleus (Freeman and Glover, 1987; Shamanski and Orr-Weaver, 1991). These previous studies did not quantitatively analyse the distribution of the asters in the absence of nuclei, and it remained unclear whether aster positioning in *gnu* mutants is a predictor of nuclear packing and order. We have shown previously that asters are required for efficient separation of daughter nuclei following chromosome segregation, and we

[1]Physics of Intracellular Organization Group, Instituto Gulbenkian de Ciência, 2780-156 Oeiras, Portugal. [2]Mechanobiology Institute, National University of Singapore, 117411 Singapore. [3]European Molecular Biology Laboratory, 69117 Heidelberg, Germany. [4]Department of Biological Sciences, National University of Singapore, 117411 Singapore. [5]Institute of Molecular and Cellular Biology, A*Star, Proteos, 138632 Singapore. [6]Warwick Medical School, University of Warwick, Coventry, CV4 7HL, UK.
*Present address: Aix-Marseille Université | AMU – Institut de Biologie du Développement de Marseille-Luminy (UMR 7288 IBDML), Case 907, Parc Scientifique Luminy, 13288 Marseille Cedex 9, France.

‡Authors for correspondence (timothy.saunders@warwick.ac.uk; itelley@igc.gulbenkian.pt)

J.d.-C., 0000-0001-7429-4193; S.T., 0000-0001-6018-9923; L.H., 0000-0002-9585-5508; T.E.S., 0000-0001-5755-0060; I.A.T., 0000-0003-4444-1046

Handling Editor: Thomas Lecuit
Received 9 July 2021; Accepted 17 December 2021

Development (2022) 149, dev199997. doi:10.1242/dev.199997

hypothesised asters pulling apart daughter nuclei (Telley et al., 2012). However, we have not addressed whether asters are necessary to maintain a regular distance to neighbouring nuclei (Kanesaki et al., 2011). Embryos lacking core centrosomal components do not regularly distribute nuclei and abort development after a few division cycles (Basto et al., 2006; Megraw et al., 1999; Vaizel-Ohayon and Schejter, 1999). Conversely, embryos that do not form actin caps and membrane furrowing, which are the precursor of uninuclear cell formation during cycle 14 and are thought to help separate nuclei at the cortex, still show regular nuclear distribution at n.c. 10 and 11 (Postner et al., 1992). The causality and the mode of mechanical separation during and after nuclear division remains an open problem, primarily due to limited visualisation in living samples and the growing mechanical complexity during development.

There have been extensive studies exploring the action of microtubules for aster or spindle centring in the early sea urchin, *Xenopus* and *Caenorhabditis elegans* embryos. These model systems represent uninuclear cells where cell geometry, cortical interactions or hydrodynamic forces appear to drive aster movement and centring, depending on species and cell context (Garzon-Coral et al., 2016; Grill et al., 2003; Meaders et al., 2020; Minc et al., 2011; Tanimoto et al., 2016, 2018; Wühr et al., 2009). A syncytium faces the need for continuous distance maintenance between neighbour nuclei in the absence of membrane boundaries. Syncytia contrast with uninuclear model systems from the point of view of complexity, though the underlying mechanism of organelle positioning could be similar (Bjerknes, 1986). In brief, how interactions between syncytial nuclei collectively generate long-ranged positional ordering remains an open challenge.

Here, we take a multiscale approach to disentangle how nuclear order emerges in the early *Drosophila* embryo. We first demonstrate that nuclear positioning and separation distance in the embryo is robust against global perturbation invoked by synchronous organelle duplication. We then show that the orientation of nuclear division displays hallmarks of short-ranged ordering within the embryo. We exploit embryonic explants (Telley et al., 2013), which reduces complexity, to explore nuclear division in a simplified system. In this system, we can dissect the principles of separation for small nuclear arrays. From this, we predict that the nuclei behave as cargo associated to self-organising microtubule asters, which we observe in explants from *gnu* mutant embryos where nuclear and centrosomal cycles are uncoupled (Freeman et al., 1986; Lee et al., 2003). We further demonstrate that nuclear ordering at low nuclear density is independent of pseudo-compartments formed by F-actin. Combining these results, we put forward a model whereby repulsive microtubule interactions between nuclei can spatially organise nuclei *in vivo*. The model correctly predicts the reorientation of neighbour nuclei observed in experiments upon sudden removal of a nucleus by laser ablation. This work provides direct evidence for the role of repulsive, short-ranged aster-driven interactions as the predominant factor in distributing and spacing nuclei evenly in the syncytial blastoderm.

RESULTS

Distance maintenance between neighbour nuclei in the *Drosophila* blastoderm

Synchronous nuclear duplication within a constant surface area poses a geometrical challenge (Fig. 1A; Movie 1). Spindle elongation during nuclear division (Telley et al., 2012) should cause transiently smaller distances between spindles (and their asters) unless some nuclei leave the surface after division, which is not observed. Because spindles are bipolar structures they could, theoretically, reorient their division axis to optimise the spacing between nuclei. A key observation is that the nuclei never collide after division, which points at a distance maintenance mechanism that is repulsive, at least at very short distances.

Thus, we wanted to better understand the local dynamics driving ordering on the *Drosophila* embryo surface. To obtain quantitative insight, we measured neighbour distances throughout division cycles 10-13, at the onset of every cycle phase (Fig. 1B,C; Fig. S1), focusing on the distance between centrosomes belonging to nearest neighbour nuclei ('non-sister' centrosomes). The internuclear distance is constant on average between divisions and undergoes a sharp reduction between anaphase onset and late anaphase, when sister chromatids are pulled apart (Fig. 1D). The spindle length expanded and shrank in each division cycle (Fig. 1E; Fig. S1). By contrast, the distance between neighbour spindle poles (non-sister centrosomes) decreased only slightly within a cycle (Fig. 1F). We estimated a phase-to-phase difference of 1-2 µm (Fig. 1G). Notably, this distance was constant between anaphase onset and late anaphase (Fig. 1G) when internuclear distance decreased (Fig. 1D). This result is remarkable given that the embryo surface area remains constant – the embryo does not grow – but spindles expand synchronously by almost 10 µm. Thus, neighbour spindle pole distances appear to be stabilised against spindle expansion and chromosome movement. In subsequent division cycles, the pattern is similar although average distances decrease gradually (Fig. S1). These measurements suggest that, despite some collective movement of nuclei (Deneke et al., 2016, 2019; Lv et al., 2020), a rigid mechanical interaction exists between neighbouring spindle poles. Thus, we hypothesised the presence of a repulsive mechanism between neighbouring nuclei or asters in the syncytial blastoderm that acts on a length scale of 5-20 µm.

Ordering of spindle orientation over short distances

In embryos at n.c. 10 and beyond, spindles have an orientation that is co-planar to the cell cortex. Within this planar topology, however, there appears to be no order in spindle orientation across the embryo (Lv et al., 2020). Despite the absence of ordered nuclear orientation across the embryo, we asked whether spindles can align across shorter distances (3-5 nuclear diameters). Such short-ranged order can have a large impact; a classic example is how subtle variations in sand corn size and shape induce small packing defects in sand piles that ultimately lead to collapse of the entire sand pile (Bak et al., 1987; Hughes and Paczuski, 2001).

In the embryo, we investigated whether there were 'chains' of aligned spindles (Fig. 2A-C; Materials and Methods). In Fig. 2B and Fig. S2A we show the definition of such 'chains': in short, two nuclei are aligned in a chain if their spindle axes are perpendicular to the vector between the two nuclei. Local alignment of spindles – which determines the division axis and future position of daughter nuclei – could be a hallmark of orientational nuclear ordering within the blastoderm. We calculated the probability of a given chain size, where size is defined by the number of nuclei belonging to the chain, L, in different cycles (Fig. 2D,E; Fig. S2) and find $P(L)\tilde{L}^{-\alpha}$. Small values of α indicate strong alignment with neighbours. In embryos $\alpha\approx2.0\pm0.3$ in n.c. 13 compared with $\alpha\approx3.6\pm0.5$ in a simulation of randomised spindle orientations. The value of α did not appear to decrease with increasing nuclear density (Fig. 2E), though it was dependent on the thresholds for defining chains (Materials and Methods; Fig. S2). Importantly, we observed clear scaling behaviour with a range of possible chain definitions, supporting that this observation is not dependent on specific

Development (2022) 149, dev199997. doi:10.1242/dev.199997

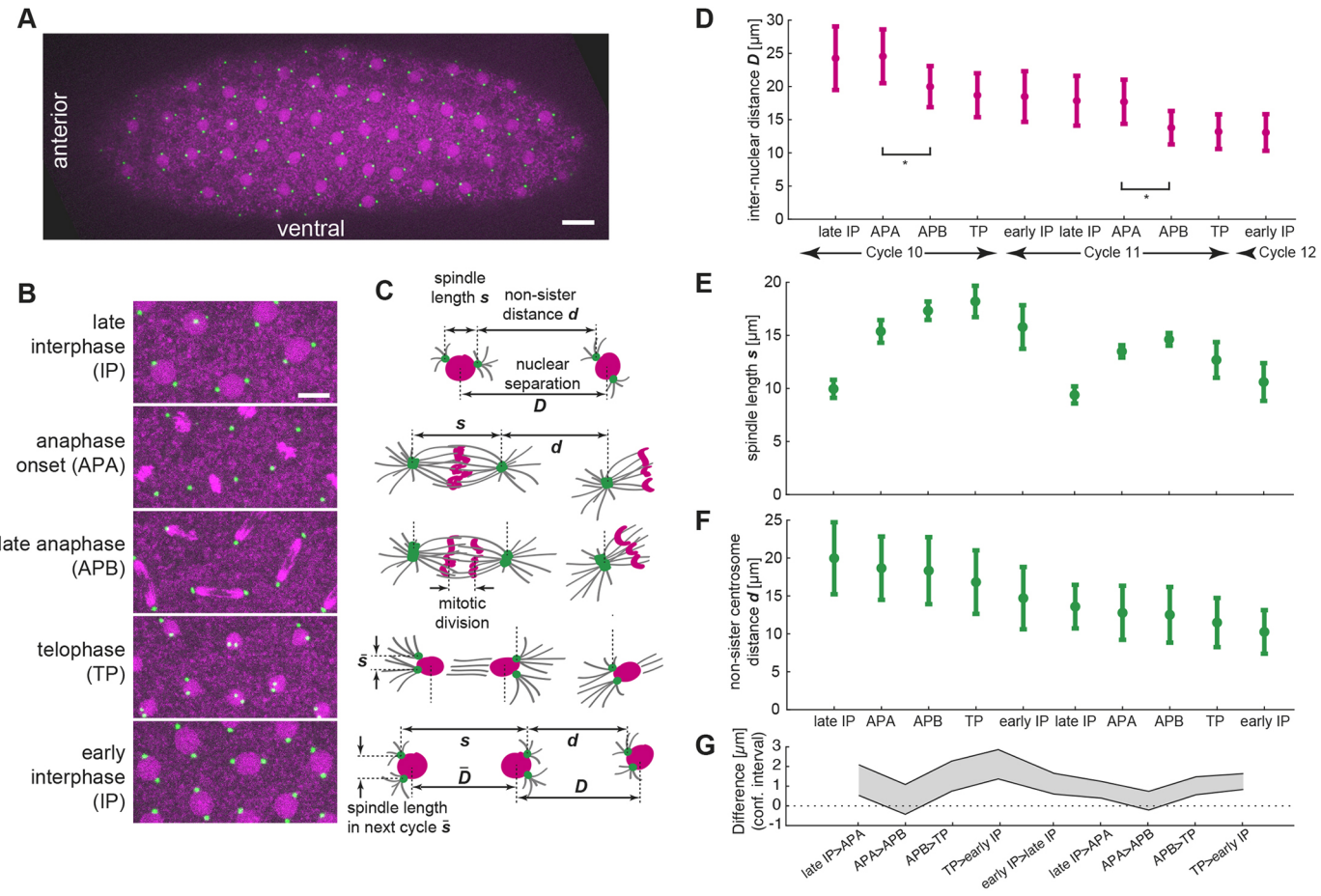

Fig. 1. Nuclear and spindle pole separation in the syncytial blastoderm of *D. melanogaster* reveal robust distance maintenance. (A) Maximum intensity *z*-projection of an embryo expressing H2Av::RFP (magenta) labelling chromatin and Spd2::GFP (green) marking centrosomes at spindle poles, taken during interphase of nuclear cycle (n.c.) 10. Anatomical orientations of the embryo are labelled. (B) Time lapse images of the embryo shown in A undergoing mitotic cleavage, showing the five phases of one cycle as labelled on the left. The label and the image represent the beginning of the respective mitotic phase. Note that, although mitosis always takes 5-6 min, interphase duration gradually increases from ∼5 min in cycle 10 to ∼16 min in cycle 13 (Crest et al., 2007). (C) Scheme of distance measurements between centrosomes or between nuclei. The scheme shows two neighbour nuclei (magenta) with associated centrosome-nucleated microtubule asters (centrosomes in green, microtubules in grey). (D) Mean±s.d. of the internuclear distance during n.c. 10 and 11, measured at the phases indicated in B (n=15 spindles in N=5 embryos). Significant difference is only detected at the transition from anaphase A to anaphase B, when sister chromatids from neighbour spindles approach each other. *P<0.05 (Student's t-test). (E) Mean±s.d. of spindle length s during n.c. 10 and 11. The plot show cyclic expansion of spindles. (F) Mean±s.d. of non-sister centrosome distance d of all first-order neighbour spindle poles. Note that this distance is relatively stable despite the spindle expansion shown in E. (G) Estimate of difference between subsequent mitotic phases (labelled at the bottom) using unpaired one-tailed Student's t-test. See also Fig. S1 and Movie 1. Scale bars: 20 µm (A); 10 µm (B).

parameter choices. The value for α is similar to the exponent in cluster size variability in a range of other physical models of short-range ordering (Chakraborty and Manna, 2014; de Gennes et al., 1995; Jo et al., 2012).

We also considered the alternative hypothesis that spindles align parallel to their axis of separation, which would be more consistent with an attractive interaction between spindles. We did observe such 'parallel chains', but with much lower frequency than the chains above; in n.c. 11, parallel chains with three or more members were three times less common than the chains shown in Fig. 2 (n=6 embryos). Further, the largest parallel chain observed in n.c. 11 had four members, compared with eight members for the chains in Fig. 2.

Thus, this new approach for analysing nuclear ordering allows us to discriminate different spindle alignments and further supports the presence of interactions between neighbouring syncytial spindles driving their division axis orientation in two dimensions while the cell cortex anchoring defines the remaining (planar) orientation. Next, we investigated the local mechanical interactions that could drive such ordering.

Nuclear positioning and division orientation in embryo explants

Studying local interactions in a large array of nuclei is challenging given that each interaction affects all its neighbours to some degree. Here, n.c. 1-2 embryos with only two or four spindles would be preferable. However, visualisation of these initial nuclear divisions, which occur deep inside the embryo, is difficult with the requisite spatiotemporal resolution. Therefore, we took advantage of an embryo explant assay, which enabled us to study a very small number of spindles in quasi-2D spaces (Telley et al., 2013) (Fig. 3A). In these explants, a single nucleus undergoes multiple rounds of division (Fig. 3B; Movie 2), and the separation between the two daughter nuclei of a division shows a characteristic length (Telley et al., 2012) similar to that measured in the embryo (Fig. 1D). We explored the relative orientation of the division axes

Development (2022) 149, dev199997. doi:10.1242/dev.199997

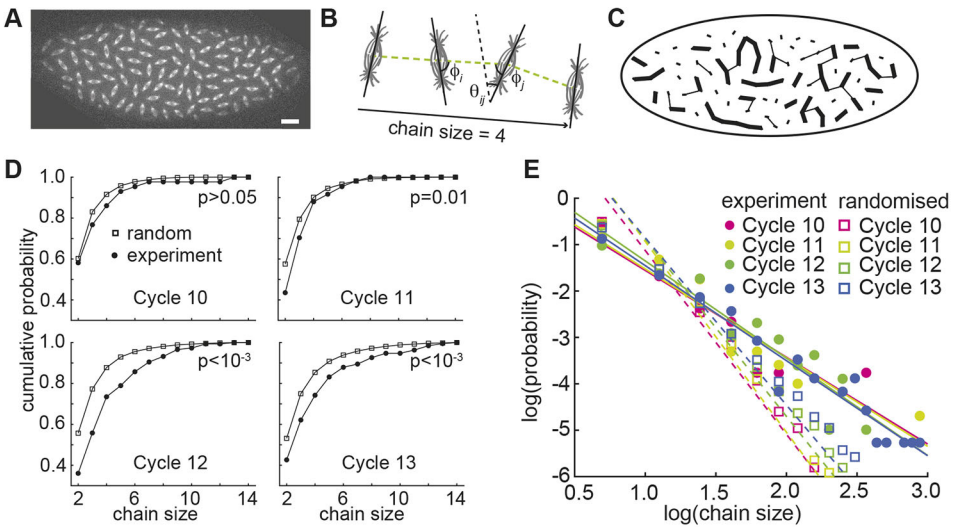

Fig. 2. Local patterns of spindle orientation in the syncytial blastoderm indicate the existence of short-range interactions. (A) Maximum intensity *z*-projection of an embryo in n.c. 11, expressing Jupiter::mCherry marking metaphase spindles. (B) The schematic illustrates neighbouring spindles belonging to an alignment ('force') chain with size (number of members) L=4. Spindles form angles θ and ϕ relative to each other (details in Fig. S2A). Spindle alignment conditions were defined for θ (weak alignment) or for both angles (strong alignment). See Materials and Methods for details. (C) Resulting alignment chains for the image shown in A; the lines denote connections that satisfy two (thick line) or only one (thin line) of the conditions defining a chain. (D) Cumulative probability function of chain size for different cycles (n=7 embryos each for n.c. 10-13). The P-value was calculated using the Kolmogorov–Smirnov test. (E) Scaling of chain size probability with chain size for n.c. 10-13. Lines represent the fit to $\beta L^{-\alpha}$, where L is the chain size and α is the scaling exponent. In D and E, we consider chains with θ and $\phi \leq \pi/4$. Fitting parameters for all conditions are presented in the Materials and Methods. See also Fig. S2. Scale bar: 20 µm.

as it is indicative of neighbour spindle interactions. When a single spindle in an explant (Fig. 3B, left) divided the nucleus, the two subsequent spindles predominantly aligned in parallel (Fig. 3B, middle). This occurred regardless of explant size and the spindle position within the explant – i.e. it did not show any clear dependence on boundary effects. However, the next round of division resulted in more disordered alignment (Fig. 3B, right; Movie 2). We also generated some explants with three spindles, either by chance during the extraction protocol or by aspiration of one of four nuclei between divisions (Fig. 3C).

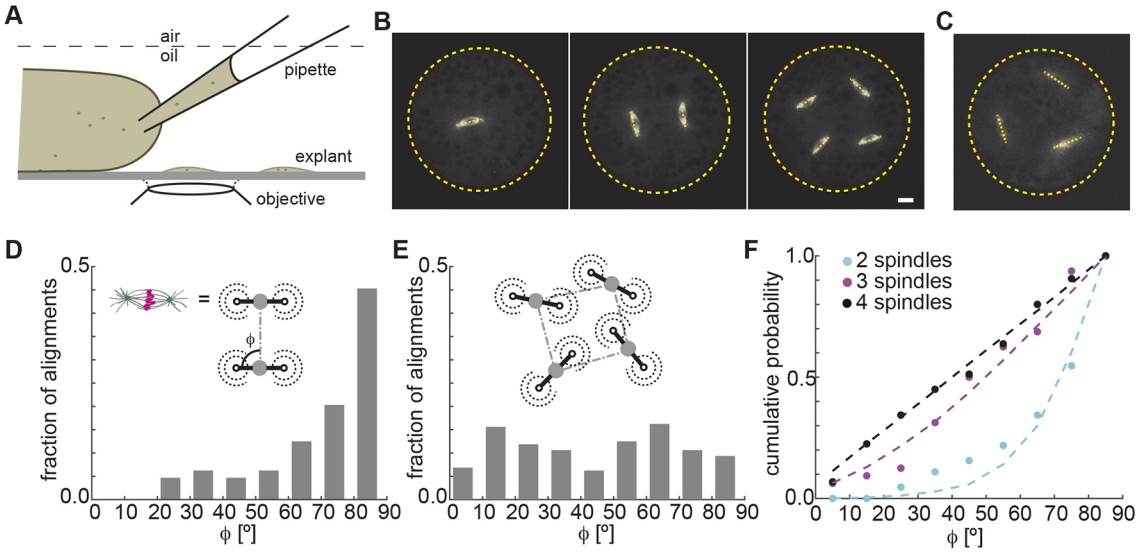

Fig. 3. Spindle axis orientations in cycling embryo explants suggest repulsion between asters of neighbouring spindles. (A) Schematic of cytosol extraction from a *Drosophila* syncytial embryo and *ex vivo* explant formation (de-Carvalho et al., 2018). (B) Fluorescence image of an explant from a single embryo expressing Jupiter::GFP (grey) containing undergoing nuclear division and different numbers of spindles. Dashed lines represent spindle axes, and yellow dashed circles represent explant boundaries. (C) Fluorescence image of an explant containing three spindles, occurring by chance during extraction. (D) Angle between the division axes of two spindles (n=32 explants). The schematic (inset) shows a spindle representing a mechanical dumbbell, and the definition of the alignment angle ϕ between the spindle axis and the line connecting neighbouring spindles: ϕ=90° for parallel spindles and ϕ=0° for spindles in line. The histogram shows a distribution towards 90° (parallel alignment). (E) Alignment angle between nearest neighbour spindles in an extract with four spindles (n=40 explants). The schematic (inset) shows a possible configuration of spindles represented by dumbbells. (F) Cumulative distribution of alignment angles for 2, 3 and 4 spindles in explants (dots). The distribution for four spindles is not significantly different from random (Kolmogorov–Smirnov test). Both two- and three-nucleus distribution is significantly different from random. Dashed lines correspond to predicted alignment of repulsive interacting asters in the presence of fluctuations (see Materials and Methods for details). See also Fig. S3A and Movie 2. Scale bar: 10 µm.

Development (2022) 149, dev199997. doi:10.1242/dev.199997

We measured spindle axis orientation ϕ relative to the separation axis (Fig. 3D, inset); parallel spindle alignment results in an angle ϕ=90°. We quantified the spindle alignment across multiple experiments for the 2-, 3- and 4-spindle scenarios. Two spindles had a strong bias towards perpendicular alignment to their separation axis (Fig. 3D). In the case of four spindles, we saw a large variety of possible spindle arrangements, with no clear bias in direction (Fig. 3E). These results were consistently reproducible across a range of nuclear positions, including when they were symmetrically distributed. For the three-spindle case, the alignment was biased away from random (P=0.04) (Fig. 3F). Here, we observed cases where one spindle was positioned out-of-plane (Fig. S3A), or two out of three spindles aligned at 90° because they were very unevenly distributed after explant manipulation. Therefore, the three-spindle results are substantially noisier than the two- and four-spindle scenarios.

In summary, we see that spindle alignment is strongly biased when two spindles are present, weakly biased with three spindles, and showing no significant bias for four spindles. Importantly, these results were obtained in explants lacking an intact cell cortex and f-actin compartments (Fig. S3B). This suggests that planar spindle orientations are not determined by cortical factors. Nevertheless, the positional order yet orientational disorder *ex vivo* is consistent with observations in embryos (see above and Kanesaki et al., 2011). The noise in the angular distribution is likely due to small deviations in nuclear position away from equidistant positions. We conclude from these observations that a dividing nucleus can be interpreted as a mechanical dumbbell, and that local interactions between spindle pole asters define separation and alignment.

Aster positioning in the absence of the nucleus

Centrosomes are essential for nuclear organisation in the embryo (Basto et al., 2006) and they remain spatially separated if DNA replication/cell division is chemically inhibited (Raff and Glover, 1989). Combining these observations with our explant results above, we posited that centrosome-nucleated asters, rather than nuclei, are the active and autonomous positioning structures in the early embryo and that is what we explored next.

To test this idea directly, we used *giant nuclei* (*gnu*) mutant embryos, which undergo DNA endoreplication without mitosis; chromosome segregation is inhibited, leading to one or few polyploid nuclei, while centrosomes continue to duplicate, separate and nucleate microtubules (Freeman and Glover, 1987; Freeman et al., 1986; Lee et al., 2003) (Fig. 4A; Movie 3). We also produced embryo explants from *gnu* mutant embryos and studied the positioning properties of a small number of microtubule asters in quasi-2D spaces. We investigated how multiple asters self-organised their position in equilibrium situations, in the absence of centrosome duplication and separation or other movement.

Notably, the inter-aster distance in *gnu* mutant embryos (Fig. 4B) at steady-state had a structural order comparable with nuclei in wild-type embryos at a similar developmental stage (Movie 3). The inter-aster distance decreased with more asters present at the embryo cortex (Fig. 4C) so that at high aster density it assumed similar values as the non-sister centrosome distance observed in wild-type embryos (Fig. 1F). Quantifying inter-aster distance along time revealed a stable and reproducible pattern in the minute time scale (Fig. 4D).

In embryo explants with precisely defined boundary conditions and specific aster numbers, the aster arrays displayed surprising levels of crystalline order (Fig. 4E). Quantifying the ordering in the three-aster droplets, we observed a bias towards equilaterally distributed asters (Fig. 4F). For four-aster droplets, 17 out of 20 droplets displayed asters in a square-like distribution (Fig. 4E), with the remaining three experiments having similar patterns (Fig. S4A). In the case that the four asters defined a quadrilateral, the average internal angle was 90°±14° (Fig. S4B); the standard deviation was much smaller than expected from randomly distributed points. This strongly suggests that neighbour asters interact with each other to generate local positional ordering, autonomous from specific embryonic signals. Unsurprisingly, the variability in aster position increased with aster number, but we still saw highly ordered, lattice-like configurations (Fig. 4E). We find similar density-dependent aster separation behaviour as observed *in vivo* (Fig. 4G). Altogether, these results argue that the asters are autonomously driving local ordering and distance maintenance within the embryo.

Of course, we must be careful in interpreting these results. Embryos from *gnu* mutants display severe defects, are arrested in their mitotic cycle and development ceases soon after the above time points. However, the striking similarity between the positional order in these mutants and the wild type is noteworthy and suggestive of a common underlying mechanism. Positional patterning of centrosome-nucleated microtubule asters in the syncytial embryo may occur largely independently from nuclei, spindle assembly, mitotic regulation and embryo cortical factors. The similarity in the structural organisation with and without nuclei supports a model that nuclei ordering is driven by local aster-aster interactions.

Positional order persists in the absence of actin pseudo-compartments

Blastoderm-stage nuclear cycles also involve the reorganisation of the actin cytoskeleton. F-actin and associated regulatory proteins are found enriched between each nucleus and the plasma membrane and it has been suggested that they form cortical domains that help position nuclei (reviewed by Schmidt and Grosshans, 2018). F-actin forms ‘caps’ that expand throughout mitosis and guide membrane invagination to form membrane furrows (Fig. 5A), which is a precursor of cellularisation (Holly et al., 2015). These furrows could assist the positional order of nuclei and define the division axes. To test this hypothesis, we quantitatively analysed nuclear positioning and division orientation in *sponge* (*spg*) mutants in which actin caps and metaphase furrows never form (Fig. 5B), and which have been reported to exhibit (qualitatively) normal nuclear positioning in n.c. 10-11 (Postner et al., 1992). In these embryos, we observed average internuclear (Fig. 5C) and non-sister centrosome (Fig. 5D) distances that are indistinguishable from wild-type embryos in n.c. 10 (Fig. 1F). Furthermore, we measured the distribution of aligned spindles in these mutants during n.c. 10. Strikingly, the observed chain distribution is similar to the wild type, with $\alpha \approx 2.45$ and different from random orientations (Fig. 5E). Therefore, in the absence of actin caps and pseudo-furrows, the nuclear alignment is as in wild type, at least during the period soon after nuclei migrate to the embryo periphery. However, we see clear aberrations from n.c. 12 onwards. This suggests that the microtubule-based distance maintenance is sufficient for spatially unconstrained syncytial divisions, whereas higher nuclear density located at the cortex requires membranous barriers for proper nuclear separation.

Relevance of aster-driven separation for nuclear packing *in silico* and *in vivo*

Our observations thus far are consistent with nuclear division axis orientation and, hence, spatial nuclear distribution being driven by short-ranged interactions between neighbouring centrosome-nucleated microtubule asters. To test this idea further, and to

Development (2022) 149, dev199997. doi:10.1242/dev.199997

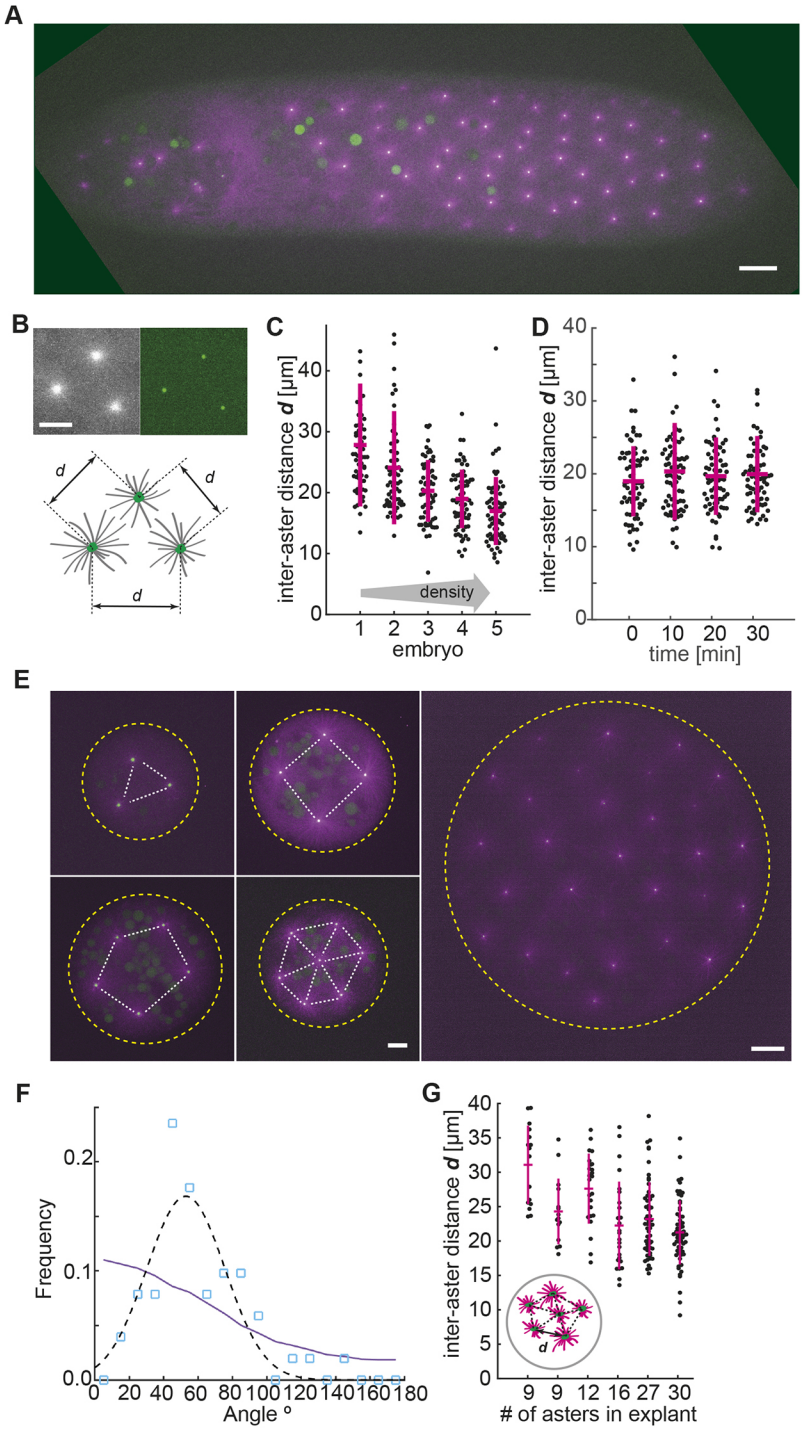

Fig. 4. Free asters in *gnu* mutant embryos dynamically position at the embryo cortex. (A) Maximum intensity *z*-projection of a *gnu* mutant embryo expressing RFP::β-Tubulin (magenta) and Spd2::GFP (green). Green circles are yolk droplets. (B) Magnification of three microtubule asters (grey) with corresponding centrosomes (green) and schematic of the measurement of inter-aster distance *d* between nearest neighbour asters (bottom). (C) Scatter plot of inter-aster distance in five embryos sorted by aster density. Black dots are individual distance measurements; mean±s.d. shown in magenta. (D) Scatter plot of inter-aster distance during consecutive intervals of 10 min for the same embryo, showing no significant change. Black dots are individual distance measurements; mean±s.d. shown in magenta. See also Fig. S3B,C and Movie 3. (E) Example images of explants from a *gnu* mutant embryo expressing RFP::β-Tubulin (magenta) and Spd2::GFP (green). The dashed yellow circle represents the explant boundary. (F) Distribution of angles between aster triplets (blue squares). Total of 51 angle measurements from 17 explants. Solid line is predicted angle distribution if aster triplets are uniformly randomly positioned within a circular geometry. Dashed line is fit of experimental data to Gaussian distribution with mean 53° and s.d. of 23°. (G) Distribution plot of inter-aster distance (*d*, see inset) of single explants of comparable size containing nine or more asters. Like in intact embryos, these explants exhibit a density dependent inter-aster distance. Black dots are individual distance measurements; mean±s.d. shown in magenta. Scale bars: 20 µm (A); 10 µm (B,E).

predict the response during perturbation experiments, we implemented an *in silico* model of nuclear separation in the embryo. Spindle alignment has been theoretically studied for uninuclear cells in other model systems and we have adopted some of these ideas (Bjerknes, 1986; Pierre et al., 2016). In our multinuclear model, the initial distribution of nuclei is taken from experimentally measured nuclear positions but initially randomised division axis orientation. Further, we allow nuclei to rotate their angle of division (Materials and Methods). A spindle was modelled as a composite of two connected asters forming a dumbbell, and each aster was taken to have a radially symmetric repulsive potential that was short-ranged (Fig. 6A). Implementing this *in silico*, we could simulate positional ordering and spindle alignment that was similar to the experimental observations (Fig. 6B). If we maintain a repulsive force between the nuclear centres, but implement an attractive potential between spindles to determine their orientation (see Materials and Methods), we see that more parallel chains are observed (Fig. 6C), inconsistent with the experimental data (Fig. 2).

We then tested the alternative model whereby an attractive interaction between asters results in a net attractive force on the nuclei position within the model. Our simulation always predicted collapse of the spindle positions to one location (Fig. 6D). This is because any irregularities in nuclear position drive the nuclei out of the steady-state distribution. In contrast, repulsive (pushing)

Development (2022) 149, dev199997. doi:10.1242/dev.199997

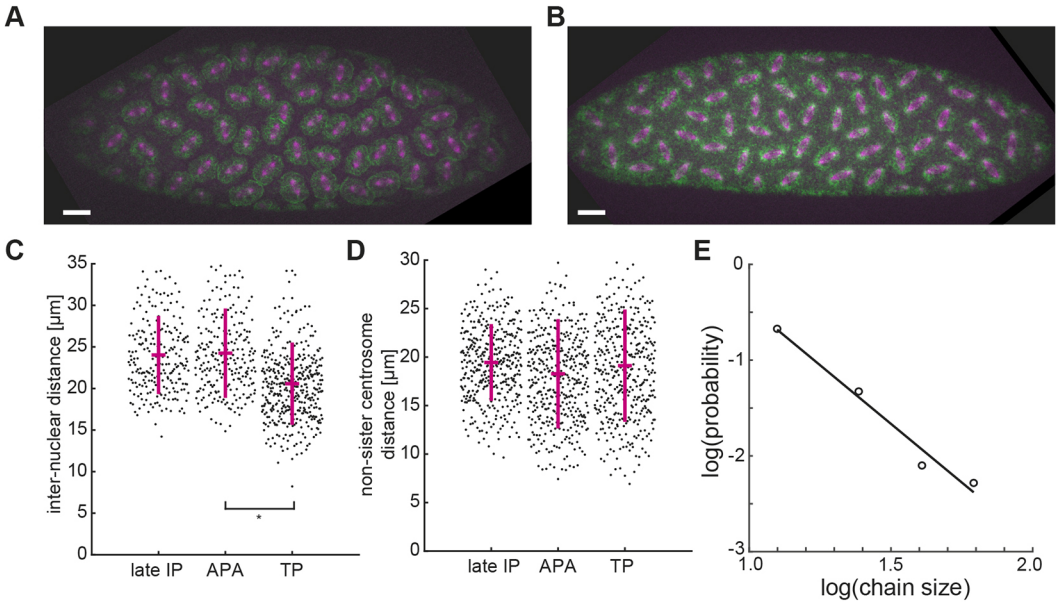

Fig. 5. Neighbour distances and spindle alignment in *spg* mutants (lacking actin pseudo furrows) are indistinguishable from wild type. (A) Maximum intensity *z*-projection of a wild-type embryo expressing Jupiter::mCherry (magenta) labelling microtubules and Utr::GFP (green) marking f-actin, taken during metaphase of n.c. 10. Note the clouds of F-actin surrounding spindles, forming cytoskeletal compartments. (B) Maximum intensity *z*-projection of a *sponge* (*spg*) mutant embryo expressing Jupiter::mCherry (magenta) labelling microtubules and Utr::GFP (green) marking f-actin, taken during metaphase of n.c. 10. Pseudo-furrows are absent in *spg* mutants but the spatial distribution of nuclei and spindles is normal in this cycle. (C,D) Scatter plots of the internuclear distance (C) and non-sister centrosome distance (D) during n.c. 10 in *spg* mutants, measured at the phases indicated. Black dots are individual distance measurements; mean±s.d. are shown in magenta (*n*=25 spindles in *N*=6 embryos). The respective mean distances are indifferent from measurements in wild type (see Fig. 1). (E) Alignment chain analysis in *spg* mutant embryos in n.c. 10. Slope of best-fit curve in log-log space α=2.45 (*n*=12 embryos), similar to Fig. 2E. IP, interphase; APA, anaphase A; TP, telophase. Scale bars: 20 µm.

interactions drive any aberrant positioned nuclei back into an equidistant arrangement. Furthermore, we could generate an array of nuclei that converged to a set of spindle orientations that show the presence of short-ranged alignment chains (Fig. 6B, highlighted regions), and we could replicate our *ex vivo* data for division orientation in 2-, 3- and 4-nuclei cases using a simplified model (Fig. 3F). To conclude, only a model with repulsive interactions between spindles which results in a net repulsive interaction between nuclei is consistent with the regular nuclear distribution within the embryo and the observed spindle orientation patterns.

Next, we asked what happens if we generate a local inhomogeneity of nuclear density? We could simulate removal of a nucleus (Fig. 6E, inset), upon which we saw reorientation of the surrounding spindles, with one spindle pole typically turning towards the newly created space (Fig. 6E). This is because the net repulsive potential in that region is decreased, favouring realignment. Our spindle alignment model suggests that even within a densely packed environment, the loss of a nucleus can result in a local reorientation of the neighbouring nuclear division axes.

We then looked to test this prediction in the early *Drosophila* embryo. Local heterogeneities in nuclear density are a common phenomenon in early embryos resulting from aberrant cortical migration or nuclear internalisation due to mitotic failure (Fig. 7A; Movie 4; Fig. S5A,B). We observed that nuclei surrounding such regions of low density had a biased orientation towards the low-density region (Fig. 7B). Repeating the same analysis on regions of uniform nuclear density showed no correlation in the division angle (Fig. S5C).

Unfortunately, small-molecule inhibitors for candidate molecular motors have no effect in *Drosophila* (Firestone et al., 2012; Maliga et al., 2002) and microtubule mutants are lethal so we cannot directly test the microtubule repulsion model *in vivo*. Therefore, to test our model predictions further we generated acute density reductions by UV ablation. Using low laser damage, the targeted nuclei failed to divide and detached from the cortex lowering local nuclear density. Subsequently, the surrounding nuclei adjusted their division axis to orientate into the perturbed region (Fig. 7C; Fig. S5D). Combining our results from spontaneous low-density regions and laser-ablated embryos (including larger ablations of 3-5 nuclei), we observed that the microtubule repulsion mechanism was efficient in adjusting the angle of division to compensate for heterogeneities in nuclear packing (Fig. 7C). Finally, we noticed a similar phenotype in *spg* mutants; when a nucleus was internalised after division failure, it left a region of low nuclear density at the cortex, and the surrounding nuclei reorientated their division axis towards this low-density region (Fig. S5E). This suggests that division axis adjustments do not emerge from the assembly/disassembly of actin caps and pseudo-furrows.

DISCUSSION

Aster positioning and spindle axis determination have been studied by cell and developmental biologists for several decades (Albertson, 1984; Gönczy et al., 1999; Hertwig, 1893; Hyman, 1989; Pflüger, 1884; Rappaport, 1961) and have seen renewed interest in recent years due to the advent of new techniques in imaging, sample control and perturbation methods (von Dassow et al., 2009; Garzon-Coral et al., 2016; Minc et al., 2011; Tanimoto et al., 2018). Aster positioning is important in egg and early embryo cells; it is at the core of pronuclear apposition after fertilisation and determines the cell division plane during early mitotic blastomere divisions (von Dassow et al., 2009; Hamaguchi and Hiramoto, 1980; Nguyen et al., 2014; Wühr et al., 2009). In eggs and embryo cells from *C. elegans* or sea

Development (2022) 149, dev199997. doi:10.1242/dev.199997

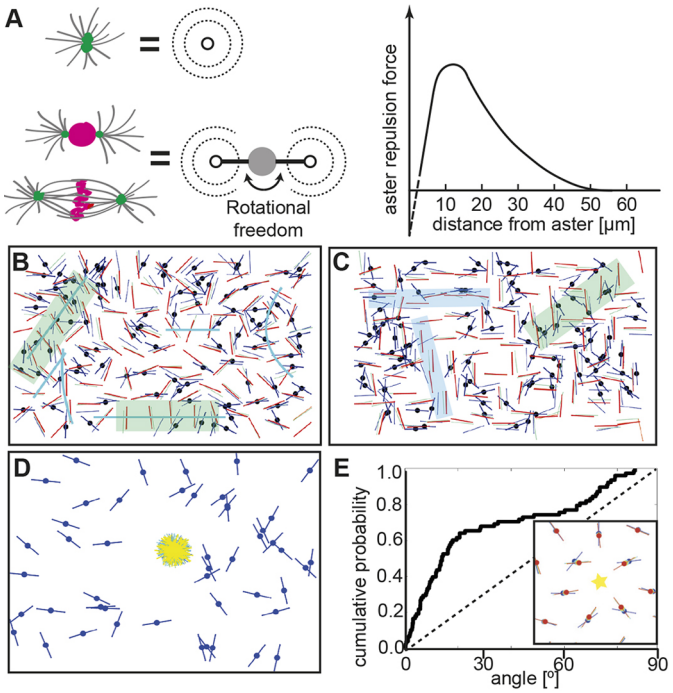

Fig. 6. Model of nuclei packing *in vivo*. (A) Schematic of repulsive potential (left). A single aster has a circularly symmetric potential. For two asters on a nucleus, they create a 'dumbbell-like' potential. Repulsive interaction is assumed to decay exponentially at long distances (>10 µm) (right). The short distance interaction (<10 µm) is not considered here as nuclei are well separated. (B) Model simulation of spindles represented as lines with central dot, carrying a short-range repulsive potential at the spindle poles (see A). Spindles are initially randomly distributed (dark blue) and reposition and align due to repulsion, as indicated by the three consecutive time points marked in light blue, green and finally red. Two chains with at least five members are highlighted by the green shaded regions. (C) As B, but with attractive interactions between spindles. Two 'parallel' chains with at least four members are highlighted with the blue shaded region. (D) Model simulation of spindles that carry a short-range attractive potential at the spindle poles, i.e. the negative of the potential shown in A ('pulling model'). Although initially randomly distributed, the spindles converge quickly to a single location. Colour code as in B. (E) Resultant spindle alignment of adjacent nuclei relative to a region of artificially low density (average from 20 simulations) made by removing a nucleus (star, inset). Inset: nuclei alignment before (blue bars) and after (red bars) nucleus removal (star).

urchin, there is evidence for cortical pulling forces positioning the mitotic spindle (Grill et al., 2003; Minc et al., 2011). However, this model does not explain observations in large cells in which repositioning occurs before astral microtubules contact the distal cell wall (Mitchison et al., 2012; Wühr et al., 2009, 2010). Sperm aster movement was initially believed to depend solely on cell wall pushing (Hamaguchi and Hiramoto, 1980). More recent studies revealed that this movement depends on cytoplasmic pulling, at the core of which is vesicle movement from the periphery towards the aster centre driven by cytoplasmic dynein (Kimura and Kimura, 2011; Tanimoto et al., 2016, 2018). In this scenario, the net force on the aster is dependent on astral microtubule length and, thus, on spatial asymmetry of microtubule density. Yet, the pulling model is currently contested by experiments that maintain support of the pushing model (Garzon-Coral et al., 2016; Meaders et al., 2020). Recent observations in *Xenopus* egg extract, either in combination with reconstituted cortical actin or exposed to artificial geometric constraints (Sulerud et al., 2020), suggest that mechanisms exist for aster positioning beyond hydrodynamic pulling (De Simone et al., 2018). In summary, cells appear to utilise a combination of possible mechanisms, depending on spatial circumstances and the process to be achieved, which then leads to a net pulling force or a net pushing force on asters. Nevertheless, all these model systems have in common that cytokinesis ensures the cytosolic isolation of individual spindles, and neighbour interactions never occur.

The mechanics of aster positioning in multinucleated cells is yet more complex, with a large array of possible interactions (Deshpande and Telley, 2021). This may be why, despite extensive previous work on nucleus positioning, the role of aster mechanics has not yet been addressed in the *Drosophila* syncytium, an otherwise popular model system in which to study development. Here, we provide clear evidence using a combination of mutant analysis, acute perturbation and a reductionist approach, that a mechanism generating net repulsion between asters has emerged, which robustly and homogenously distributes syncytial nuclei.

Robust embryonic development depends on homogenous delivery of nuclei to the cell cortex and subsequent maintenance of a regular nuclear distribution despite further division cycles (Hatanaka and Okada, 1991; Zalokar and Erk, 1976). Recent work has shown how nuclear divisions are synchronised and, consequently, how nuclei are globally distributed around the embryo cortex (Deneke et al., 2016, 2019). However, these results assumed that nuclei are positioned regularly after each round of duplication. Although there has been extensive modelling for positioning in uninuclear cells, a systematic analysis of how multiple nuclei position within a syncytium is much less explored. Here, we used quantitative *ex vivo* and *in vivo* approaches to dissect the mechanical processes ensuring such local order of nuclei. To tackle this challenge required understanding the biophysical principles defining spindle axis orientation, and how nuclei separate and reposition during division cycles. Our explant experiments demonstrate that, in the absence of perturbation by neighbour interactions, the fundamental orientation of a spindle is orthogonal to the previous division axis (Fig. 3). Our results can be explained by the stereotypical migration of the two centrosomes from their common origin, each along one quadrant of the nucleus, until they form the poles of the bipolar spindle (Robinson et al., 1999). Hence, orthogonality of spindle axes likely emerges from the geometric nature of bipolar structures and symmetry considerations. Surprisingly though, a system of four or more spindles in a two-dimensional space evolves towards random orientations, arguing against active spindle orientation control by the cell, though short-ranged local order can occur (Fig. 2) due to localised inhomogeneities in nuclei distribution. Our analysis suggests that force balance and energetic minimisation in a noisy two-dimensional environment (Fig. 6) dynamically determine where nuclei are positioned and in which orientation they propagate upon division.

Interestingly, in larger networks, small positional irregularities result in division axis orientation towards the low-density region (Fig. 7), enabling the nuclear distribution to homogenise quickly and act as a self-repair mechanism. Of course, *in vivo* the asters interact in three-dimensions and the nuclei also have two rotational degrees of freedom. However, given the positioning constraints due to nuclear anchoring at the embryo cortex during n.c. 10-13, our explant results are likely a good approximation to the *in vivo* interaction. Finally, it would be interesting to compare aster force driving spindle alignment in the early embryo with similar microtubule-driven processes across cells, such as mitosis in polarised tissue growth (Nestor-Bergmann et al., 2014).

Dissecting the molecular mechanism of microtubule aster repulsion in the embryos by genetic manipulation is challenging as many microtubule-associated proteins and motors play an

Development (2022) 149, dev199997. doi:10.1242/dev.199997

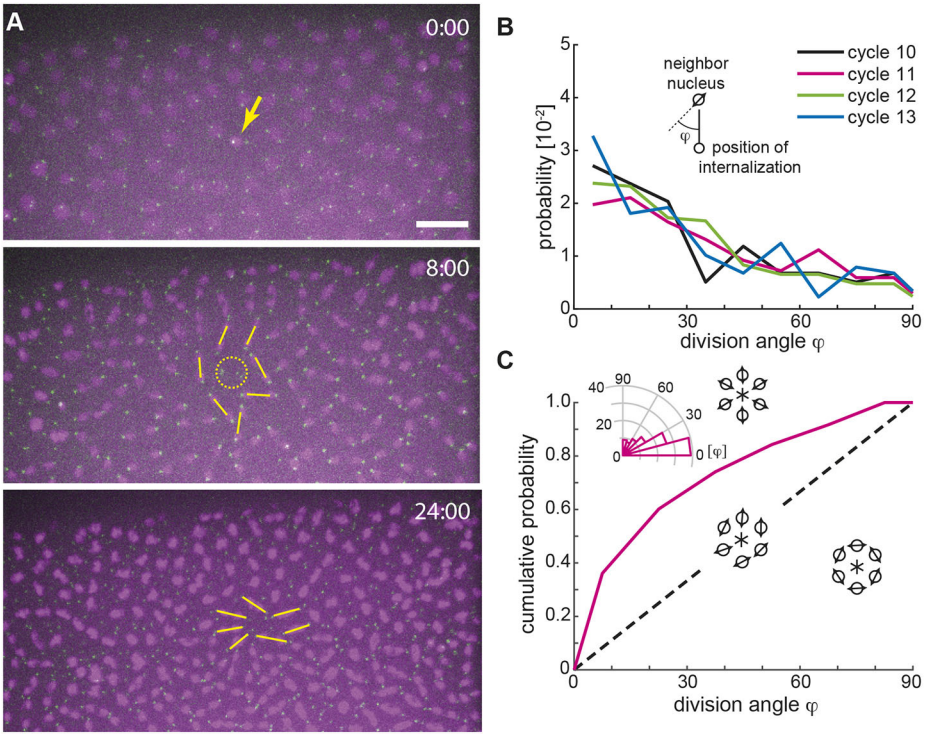

Fig. 7. Microtubule-dependent repulsion provides a mechanism for spindle alignment towards lower density. (A) Maximum intensity *z*-projections from an embryo expressing H2Av::mCherry (magenta) and Spd2::GFP (green) in n.c. 12-13. Yellow arrow (top panel) denotes internalisation of a nucleus. The centrosomes remain at the embryo cortex (yellow circle, middle panel). Division axes of neighbouring spindles (yellow lines) orientate towards the location of internalisation in n.c. 13 (bottom panel). Time in min:sec. (B) Probability density function of the division angle orientation ϕ of neighbouring nuclei to regions of low nuclear density in n.c. 10-13 (*n*=67, 116, 96, 73 angles from *N*=10, 15, 15, 15 embryos in n.c. 10, 11, 12, 13, respectively). (C) Cumulative distribution function of division axis angle at the end of n.c. 13 towards artificially generated holes created by single-pulse UV laser ablation (*n*=108 angles from 15 embryos). The dashed black line represents random division orientation. See also Fig. S4 and Movie 4. Scale bar: 20 µm

essential role during oogenesis and early embryogenesis. Moreover, unlike in other species, available small-molecule inhibitors do not specifically target these motors in *Drosophila* (Firestone et al., 2012; Maliga et al., 2002). Alternative approaches have been used, such as antibody-mediated inhibition, TEV-mediated protein cleavage or germline-specific RNAi. Inhibition of Klp61F, a promising candidate for driving microtubule-based repulsion (Baker et al., 1993), causes a strong spindle assembly phenotype in syncytial embryos (Sharp et al., 1999). In combination with knockdown of the antagonising Ncd (kinesin-14), spindle assembly was rescued but spindles and daughter nuclei failed to separate properly (Sharp et al., 1999). In a transgenic Klp61F null construct expressing TEV-Klp61F-GFP, nuclei were more disordered in interphase following injection of TEV, which chemically ablates the motor (Lv et al., 2018). However, the authors doubted microtubule sliding of Klp61F being essential for nuclear positioning as they recorded higher mobility of nuclei after TEV injection. Recently, we have shown that Fascetto (Feo), a microtubule crosslinker of the PRC1/Ase1 family, and Klp3A (Kinesin-4) colocalise as puncta in regions between neighbouring nuclei. Depletion of Feo leads to irregular delivery of nuclei to the cortex and loss of separation after nuclear repositioning by micro-manipulation (Deshpande et al., 2021). Is the observed aberrant nuclear movement and positioning in the syncytial embryo of the above mutants due to pushing or pulling forces, and what role does the nucleus play? In the present study, we provide evidence that there exists mechanical repulsion between asters independent of the nucleus and cell cortex.

Why is a high spatial regularity of nuclei important for the embryo? After n.c. 13, the embryo transforms into a multicellular embryo by engulfing each nucleus with plasma membrane (Lecuit and Wieschaus, 2000). During this process, the nearest neighbour internuclear distance defines cell size. Therefore, a narrow distance distribution leads to a uniform size of cells that subsequently assume distinct function during body part definition. Analysis of information decoding in the *Drosophila* embryo has shown how each individual cell unambiguously reads its current position, which defines a specific function later in development (Petkova et al., 2019). But these results are dependent on the interpreting units (i.e. the nuclei) being uniformly distributed around the embryo. Therefore, we can conclude that a robust mechanism defining cell size and position is crucial as size irregularity would effectively decrease positional precision.

MATERIALS AND METHODS

Fly strains

Flies with genotypes w^{1118}; +; endo>Jupiter::GFP [stock no. 6836, Bloomington *Drosophila* Stock Center (BDSC)] and w*; +; endo>H2Av::RFP (stock no. 23650, BDSC) were crossed to generate recombinant progeny. Similarly, flies expressing fluorescent reporters recombined on the second chromosome were produced by crossing the following stocks: w*; endo>H2Av::RFP;+ (stock no. 23651, BDSC) | w*; pUbq> β-Tubulin::EGFP;+ (stock no. 109603, Kyoto Stock Center) | w*; pUbq>RFP::β2-Tubulin;+ [originally described in Inoue et al. (2004)] | w^{1118}; pUbq>Spd2::GFP;+ (gift from Mónica Bettencourt Dias, Instituto Gulbenkian de Ciência, Portugal). All resulting recombinant fly lines are homozygous viable. H2Av::mCherry flies were generated as previously described (Krzic et al., 2012). w^{1118}; +; Jupiter::mCherry was generated by and obtained from Nick Lowe in Daniel St. Johnston's lab (The Gurdon Institute, UK). w^{1118}; +; sqh>UtrABD::GFP/TM3,Sb was a gift from Matteo Rauzi (Institut de Biologie Valrose, France) and originally made by R. Levayer (Rauzi et al., 2010). These two fly lines were recombined on the third and balanced on the second chromosome resulting in: w^{1118}; CyO/Sco; sqh>UtrABD::GFP, Jup::mCherry/TM6B.

Two different mutants of giant nucleus (*gnu*), namely w*; +; gnu^{305}/TM3 (discontinued stock no. 3321; BDSC) and w*; +; $gnu^{Z3\text{-}3770A}$/TM3 (discontinued stock no. 38440; BDSC), were each balanced with w^{1118}; CyO/Sco; MKRS/TM6B (stock no. 3703, BDSC). Above-described recombined lines on the second chromosome were individually crossed with *gnu* mutants and kept as balanced stocks. Finally, trans-heterozygous were generated for $gnu^{305}/gnu^{Z3\text{-}3770A}$ mutants, whereby only flies

Development (2022) 149, dev199997. doi:10.1242/dev.199997

homozygous for the fluorescent reporters on the second chromosome were selected for increased signal collection during live microscopy. These trans-heterozygotes laid fertilised eggs which undergo several embryonic rounds of chromatin replication and centrosome duplication, allowing for the study and quantification of asters at the embryo cortex.

The sponge (*spg*) mutant lines were a gift from E. Wieschaus (Princeton, USA): spg805 12 recombinant/TM3,Sb and HisGFP-H2A, e, spg242/TM3, Sb. The first was recombined on the third chromosome to obtain w^{1118}; CyO/Sco; spg805, sqh>UtrABD::GFP, Jup::mCherry/TM6B. The second was crossed to w^{1118} to recombine out the HisGFP-H2A and generate w1118; +; e, spg242/TM3,Sb. By simple cross, we then generated heterozygous females of spg805/spg242 expressing Utr::GFP and Jup::mCherry. As a control, we obtained a deficiency line for sponge, Df3450 (gift from Eyal Schejter and Benny Shilo, Weizmann Institute, Israel, BDSC #430), and generated heterozygous females of spg805/Df3450 expressing Utr::GFP and Jup::mCherry. Both these heterozygous constructs showed the same phenotype.

Embryo collection and sample preparation

We followed established procedures (Schubiger and Edgar, 1994) of fly husbandry, keeping flies at 25°C under 50-60% humidity. For embryo collections, young adult flies were transferred to a cage coupled to an apple juice agar plate. After 2-3 rounds of egg laying synchronisation, developing embryos were collected every 30-60 min. In the case of *gnu* mutants, embryos were collected at different time intervals, ranging from 30 min up to 4 h. Embryos were dechorionated by short immersion in 7% sodium hypochlorite solution (VWR). After extensive rinsing with water, embryos were aligned and immobilised in a thin strip of heptane glue placed on 22×22 mm coverslips, and covered with halocarbon oil (Voltalef 10S, Arkema).

Microscopy

Time-lapse acquisitions were conducted on a Nikon Eclipse Ti-E microscope equipped with a Yokogawa CSU-W Spinning Disk confocal scanner and a piezoelectric stage (737.2SL, Physik Instrumente). For embryo imaging, 15 µm (31 planes) Z-series stacks were acquired every 15 s (wild type, if not stated otherwise) or 30 s (*gnu* mutant), using a Plan Fluor 40×1.3NA oil immersion objective, the 488 nm and 561 nm laser lines, and an Andor Zyla 4.2 sCMOS camera to acquire images. For explants up to 100 µm in diameter, we used a Plan Apo VC 60×1.2NA water immersion objective with 2× post-magnification and an Andor iXon3 888 EMCCD camera. When needed, the Andor Zyla 4.2 sCMOS camera was selected to acquire a 2× wider field of view with the same spatial resolution or, alternatively, the Apo λ S LWD 40×1.15NA water immersion objective. For acquisition in explants, the frame rate was 15 s for *gnu* mutant and 30 s for wild-type embryo explants.

Single embryo explant assay

Embryo extractions were performed as previously described (de-Carvalho et al., 2018; Telley et al., 2013). Briefly, cytosol from wild-type embryos between telophase and subsequent interphase of cycle 8 was extracted by puncturing the vitelline membrane with a sharp glass micropipette and flow controlled by operating a bi-directional syringe pump. Small explants of cytosol (in the picolitre range) were deposited on poly-L-lysine-coated glass surface under halocarbon oil. Time-lapse acquisitions typically started in late interphase or prophase. In the case of *gnu* mutant embryos, most extractions were performed when few centrosomes (between 5 and 40) were visible at the anterior-lateral cortex. During extractions, shear stress was avoided to prevent structural damage and undesirable molecular dissociations that induce premature mitotic failures or aberrant microtubule structures. In *gnu* mutant embryos, repeated use of the same extraction micropipette is not recommended. Explants from wild-type embryos initially containing a single nucleus were selected for time-lapse imaging of subsequent mitotic divisions. Explants from *gnu* mutants initially containing a single free aster near the oil interface or two free asters in close proximity were selected for time-lapse imaging of aster separation. All experiments were conducted at 25±1°C.

Laser ablation system

The laser ablation systems used for experiments with intact embryos (at EMBL Heidelberg; Telley et al., 2012) and embryo extracts (at Instituto Gulbenkian de Ciência, implemented by I.A.T. on the microscope described above) were conceptually identical. A Crylas FTSS-355-Q pulsed laser emitting 355 nm, 1.1 ns pulses, 15 µJ pulse energy at 1 KHz was aligned with a beam expander (16×), a scan head (SCANcube 7, Scanlab) coupled to an f-theta lens (f=56 mm, anti-reflection coating for 340–370 nm, Scanlab). The focus point of the f-theta lens was aligned to be parfocal to the focal plane of the objective, using a tube lens (f=200 mm, Ø=30 mm, 355 nm AR coated, OWIS) and a dichroic mirror (T387 DCLP, Chroma) in the upper stage filter wheel. Any scattered light was blocked at the emission side with a RazorEdge LP 355 dichroic mirror OD6 at 355 nm (Chroma). The system was controlled with homemade journals for Metamorph software (Molecular Devices). The optimal laser power was set to ensure microtubule ablation while avoiding thermal expansion of cytoplasm, with post-ablation microtubule signal recovery matching known polymerisation dynamics. This combination of conditions proved to be efficient at ablating target structures beyond fluorophore bleaching.

Distance analysis in embryos

Automated positional detection of the signals from centrosomes and nuclei (or chromatin) was performed by applying a Gaussian blur filter (radius: 1-2 pixels) and using the plugin TrackMate v3.5.1 in Fiji ImageJ (Schindelin et al., 2012; Tinevez et al., 2017). The coordinates of detected spots were imported into Matlab® for assignment and distance calculation. The connection between poles belonging to a spindle structure was assigned in a custom-made script requiring user input, on an area containing 15-40 spindles for each mitotic phase and per embryo. For each spindle-assigned coordinate position, the nearest neighbour positions were determined using the Delaunay triangulation functions in Matlab® yielding a connectivity list. Thereby, a spindle structure is defined as a combination of n centrosome and m chromatin positions (n,m) with the following numbers for mitotic phases: late interphase (2,1); anaphase A (2,1); anaphase B (2,2); telophase (4,2), early interphase (4,2). With this assignment, the duplicated organelles dissociate at the transition from telophase to early interphase, so that two related nuclei become independent neighbours. Next, the 3D Euclidean distances between relevant positions were calculated from position coordinates with a computer-assisted manual heritage classification. The distance between separating chromosomes $\bar{D}$ was calculated from the two chromatin entities within a spindle. Spindle length s was calculated from the distance between two centrosomes belonging to each spindle. In phases with four centrosomes per spindle, two at each pole, spindle length was defined as the smallest distance between opposite centrosomes (four possible combinations). The sister centrosome distance $\bar{s}$ was calculated from centrosome pairs at each spindle pole. Inter-aster distance d (corresponding to the distance between non-sister centrosomes) was calculated between different, neighbouring spindles by selecting all centrosomes not associated with the same spindle from the nearest neighbour connectivity list. Internuclear distance D was calculated between nearest neighbour nuclei or chromosomes not belonging to the same spindle. Finally, the arithmetic mean and standard deviation of the distance distributions within a single embryo were calculated and overlaid for division cycles 10-13; all mean values are shown in Fig. S1. In *gnu* mutant embryos, inter-aster distance d_a was calculated from a selected region containing 15-20 centrosomes, for each embryo at different time points using triangulation and neighbourhood connectivity list. Centrosomes located at the anterior hemisphere were excluded to avoid the influence of the giant polyploid nucleus. The *gnu* mutants present variable centrosome densities depending on age and other unknown factors. We analysed the variation of distance distribution for five different embryos with similar densities during intervals of 10 min. All data plots were generated in Matlab®.

Spindle alignment in explants

Extracts initially containing two, three and four dividing nuclei were analysed in terms of spindle axis orientation by analysis of microtubule reporters at the onset of anaphase B. Using Matlab® homemade scripts, the

Development (2022) 149, dev199997. doi:10.1242/dev.199997

two minor orthogonal angles (ϕ_1 and ϕ_2) were determined by manual clicking at spindle poles. These angles can range between 0° (parallel orientation) and 90° (perpendicular orientation).

The angle analysis for aster-triplets in the explants was performed using the angle operation in Fiji. Seventeen explant experiments were analysed, with three angles extracted from each experiment. To check for measurement error, we confirmed that the sum of these three angles was within 2% of 180° for every explant (average error<0.7%). For four-aster scenarios where the asters arranged in a quadrilateral arrangement, we measured the four internal angles of the defined quadrilateral (Fig. S4B). We ensured that the measured angles for each quadrilateral summed to 360°±5°.

Dumbbell model of nuclear alignment in explants

For Fig. 3F, we considered a simple phenomenological model: $H = J\sum_{\langle i,j\rangle}(\vec{S_i}\cdot\vec{r}_{i,j})^2$, where $\vec{S}_i$ represents the orientation of aster i (with $|S_i|$=1) and $\vec{r}_{i,j}$ is the unit vector between aster i and its nearest neighbours j. The model is quadratic as there is no preferential direction for S. In this case, energy is minimised if nuclei align perpendicular to the vector of separation, $\vec{r}_{ij}$, between nuclei, consistent with the two-nuclei case. In the case of two nuclear spindles, it is clear this results in parallel aligned nuclear spindles, both of which are perpendicular to the vector between the nuclei. For three spindles, positioned at (0,0), (1,0) and (1/2, $\sqrt{3}$/2), the energy is minimised for $S_1 = \left(-\frac{1}{2},\frac{\sqrt{3}}{2}\right)$, $S_2 = \left(\frac{1}{2},\frac{\sqrt{3}}{2}\right)$ and $S_3 = (1, 0)$ (direction of the vectors can also be inverted). For a square, $\vec{r}_{12} = (1,0)$, $\vec{r}_{13} = (0,1)$, $\vec{r}_{24} = (0,1)$, $\vec{r}_{34} = (1,0)$ (note we do not consider $\vec{r}_{14}$ and $\vec{r}_{23}$ as these vertices are not nearest neighbours). We consider two demonstration cases. Consider all vectors S_i = (1, 0). In this case, $H = J(1^2+0^2+1^2+0^2+0^2+1^2+0^2+1^2) = 4J$ (i.e. each vector S lies parallel and perpendicular to one side of the square). Next, consider $S_2 = \left(\frac{1}{\sqrt{2}},\frac{1}{\sqrt{2}}\right)$, $S_2 = \left(\frac{1}{\sqrt{2}},\frac{1}{\sqrt{2}}\right)$, $S_3 = \left(\frac{1}{\sqrt{2}},\frac{1}{\sqrt{2}}\right)$ and $S_4 = \left(\frac{1}{\sqrt{2}},-\frac{1}{\sqrt{2}}\right)$ (i.e. each vector S is orientated perpendicular to the direction to the centre of the square). In this case

$$H = J\left[\left(\frac{1}{\sqrt{2}}\right)^2+\left(-\frac{1}{\sqrt{2}}\right)^2+\left(\frac{1}{\sqrt{2}}\right)^2+\left(\frac{1}{\sqrt{2}}\right)^2+\left(\frac{1}{\sqrt{2}}\right)^2+\left(\frac{1}{\sqrt{2}}\right)^2+\left(\frac{1}{\sqrt{2}}\right)^2+\left(-\frac{1}{\sqrt{2}}\right)^2\right] = 4J.$$

Both orientations have the same energy term, which contrasts with the two- and three-spindle cases where there are angle preferences.

We used a Metropolis algorithm to simulate the alignment of asters at different effective temperatures T. Of course, in this highly active system thermal fluctuations are likely substantially less important than other sources of noise. Hence, the T here is an effective temperature used to introduce noise into the simulations, not reflective of actual temperature fluctuations. There is only one parameter, defined by J/k_BT, which represents the competition between alignment forces and random fluctuations. Results presented in Fig. 3F are for $\frac{J}{k_BT} = 10^{-1}$. Of course, we can consider more complex models, such as

$$H = J\sum_{\langle i,j\rangle}(1-(\vec{S}_i\cdot\vec{S}_j)^2)(\vec{S}_i\cdot\ \vec{r}_{i,j})^2,$$

which incorporate both terms involving neighbouring aster alignment and their alignment relative to $\vec{r}_{ij}$. There is also similarity to models of nematic ordering in liquid crystals (de Gennes et al., 1995), which have recently been applied to other biological systems (Saw et al., 2017). Studies of self-propelled particles with repulsive interactions are also relevant, where longer-ranged interactions are also considered (Menzel and Ohta, 2012). Our aim here is to simply show how simple dumbbell-like repulsion (which results in one rotational degree of freedom) can lead to different behaviours depending on the system topology, and not to build a precise model for how such potentials interact.

Dynamic model of aster interactions

The cytoplasm is viscous. For a viscous material, the velocity, v, of an object is dependent on the applied force F: $v \approx \gamma F$, where γ is the effective viscous drag coefficient. In our simple dynamic model implemented in Matlab® we consider γ=1 (as the precise value is only a linear fitting parameter and does not change the system behaviour) and isolated asters with a radially symmetric force potential described by $F(r)=e^{-r/\lambda}$, where r is the distance from the aster centre (centrosome) (Fig. 6A). The sign of the force potential defines repulsion (+) or attraction (−).

We implemented our model of aster repulsion to spindle alignment in the embryo (Fig. 6B). In this case, we implemented periodic boundary conditions as the embryo is ellipsoidal, and nuclei position was initiated with similar density to the experiment (Fig. 6B). The dynamics of the barycentre of each spindle was determined as in the dynamic model of aster separation described above. The dynamics of reorientation of each spindle was determined by the coupling between the spindle orientation – defined by an angle θ_i between −90 and 90 degrees – and the orientation of the axis connecting each spindle barycentre to the barycentre of its neighbouring spindles – defined by an angle θ_{ij} between −90 and 90 degrees. The dynamic equation for θ_i is

$$\frac{d\theta_i}{dt} = a_0 * \sum_{j=0}^{n} \mathrm{sign}(\theta_i-\theta_{ij}) * \cos(\theta_i-\theta_{ij}) e^{-r/\lambda},$$

where the sum is over nearest neighbours for spindle i. For Fig. 6C, we altered the cos function to a sin function, which represents attractive interactions between neighbouring spindles.

For repulsive interactions, we allowed the system to equilibrate and then simulated ablation by removing a nucleus instantaneously. We then recorded the dynamic changes in aster alignment after ablation (Fig. 6E).

Analysis of nuclei internalisation in embryos – angle probability distributions from laser ablation experiments

Embryos expressing H2Av::mCherry were segmented using level sets and watershed algorithms in Matlab®. Regions of low nuclear density were identified as pixels that were positioned greater than 20% of the average nucleus separation from the nearest nucleus (Fig. S4A,B). The centre of mass of the low-density region was identified. The division angle orientation ϕ of the neighbouring nuclei was measured relative to the centre of mass. Therefore, a nucleus dividing directly into the region of low density would be assigned an angle of 0°, and a nucleus dividing perpendicular to the region would be assigned an angle of 90°. As the division does not have a preferred direction, the angle range is between 0° and 90°. A similar analysis was performed for the laser ablations, where the centre of the low-density region (artificially generated by ablating nuclei) was used to determine the relative angle of the division axis for the neighbouring nuclei.

Acknowledgements

We thank members of the I.A.T. and T.E.S. labs for fruitful discussions, and Virgile Viasnoff, Gianluca Grenci, Tetsuya Hiraiwa, Jacques Prost and Thomas Surrey for constructive comments and feedback. We thank the staff of the Fly Facility, the Advanced Imaging Facility (AIF) and the Technical Support Service at the Instituto Gulbenkian de Ciência. Transgenic fly stocks were obtained from BDSC (National Institutes of Health).

Competing interests

The authors declare no competing or financial interests.

Author contributions

Conceptualization: J.d.-C., T.E.S., I.A.T.; Methodology: J.d.-C., T.E.S., I.A.T.; Software: L.H.; Validation: J.d.-C., S.T., T.E.S., I.A.T.; Formal analysis: J.d.-C., S.T., T.E.S., I.A.T.; Investigation: J.d.-C., S.T., T.E.S., I.A.T.; Resources: L.H., T.E.S.; Writing - original draft: J.d.-C., T.E.S., I.A.T.; Writing - review & editing: T.E.S., I.A.T.; Visualization: J.d.-C., S.T., T.E.S., I.A.T.; Supervision: T.E.S., I.A.T.; Project administration: I.A.T.; Funding acquisition: T.E.S., I.A.T.

Funding

We acknowledge financial support from: Human Frontier Science Program (HFSP) awarded to I.A.T. and T.E.S. and supporting J.d.-C. and S.T. (RGY0083/2016); Fundação Calouste Gulbenkian (FCG); the Fundação para a Ciência e a Tecnologia (FCT) supporting I.A.T. (investigador FCT IF/00082/2013); EU FP7

People: Marie-Curie Actions 2013-CIG (N° 818743) awarded to I.A.T. and supporting J.d.-C.; LISBOA-01-0145-FEDER-007654 supporting Instituto Gulbenkian de Ciência (IGC) core operations, LISBOA-01-7460145-FEDER-022170 (Congento) supporting the IGC Fly Facility, PPBI-POCI-01-0145-FEDER-022122 supporting the IGC AIF, all co-financed by FCT (Portugal) and Lisboa Regional Operational Program (Lisboa2020) under the PORTUGAL2020 Partnership Agreement (European Regional Development Fund).

Peer review history

The peer review history is available online at https://journals.biologists.com/dev/article-lookup/doi/10.1242/dev.199997.

References

Albertson, D. G. (1984). Formation of the first cleavage spindle in nematode embryos. *Dev. Biol.* **101**, 61-72. doi:10.1016/0012-1606(84)90117-9

Bak, P., Tang, C. and Wiesenfeld, K. (1987). Self-organized criticality: an explanation of the 1/ f noise. *Phys. Rev. Lett.* **59**, 381-384. doi:10.1103/PhysRevLett.59.381

Baker, J., Theurkauf, W. E. and Schubiger, G. (1993). Dynamic changes in microtubule configuration correlate with nuclear migration in the preblastoderm Drosophila embryo. *J. Cell Biol.* **122**, 113-121. doi:10.1083/jcb.122.1.113

Basto, R., Lau, J., Vinogradova, T., Gardiol, A., Woods, C. G., Khodjakov, A. and Raff, J. W. (2006). Flies without Centrioles. *Cell* **125**, 1375-1386. doi:10.1016/j.cell.2006.05.025

Bjerknes, M. (1986). Physical theory of the orientation of astral mitotic spindles. *Science* **234**, 1413-1416. doi:10.1126/science.3787253

Callaini, G. and Riparbelli, M. G. (1990). Centriole and centrosome cycle in the early Drosophila embryo. *J. Cell Sci.* **97**, 539-543. doi:10.1242/jcs.97.3.539

Chakraborty, A. and Manna, S. S. (2014). Space-filling percolation. *Phys. Rev. E* **89**, 032103. doi:10.1103/PhysRevE.89.032103

Crest, J., Oxnard, N., Ji, J.-Y. and Schubiger, G. (2007). Onset of the DNA replication checkpoint in the early Drosophila embryo. *Genetics* **175**, 567-584. doi:10.1534/genetics.106.065219

de-Carvalho, J., Deshpande, O., Nabais, C. and Telley, I. A. (2018). A cell-free system of Drosophila egg explants supporting native mitotic cycles. *Methods Cell Biol.* **144**, 233-257. doi:10.1016/bs.mcb.2018.03.011

de Gennes, P. G., Prost, J. and Pelcovits, R. (1995). The physics of liquid crystals. *Phys. Today* **48**, 70-71. doi:10.1063/1.2808028

De Simone, A., Spahr, A., Busso, C. and Gönczy, P. (2018). Uncovering the balance of forces driving microtubule aster migration in C. elegans zygotes. *Nat. Commun.* **9**, 938. doi:10.1038/s41467-018-03118-x

Deneke, V. E., Melbinger, A., Vergassola, M. and Di Talia, S. (2016). Waves of Cdk1 activity in S phase synchronize the cell cycle in Drosophila embryos. *Dev. Cell* **38**, 399-412. doi:10.1016/j.devcel.2016.07.023

Deneke, V. E., Puliafito, A., Krueger, D., Narla, A. V., De Simone, A., Primo, L., Vergassola, M., De Renzis, S. and Di Talia, S. (2019). Self-organized nuclear positioning synchronizes the cell cycle in Drosophila embryos. *Cell* **177**, 925-941.e17. doi:10.1016/j.cell.2019.03.007

Deshpande, O. and Telley, I. A. (2021). Nuclear positioning during development: pushing, pulling and flowing. *Semin. Cell Dev. Biol.* **120**, 10-21. doi:10.1016/j.semcdb.2021.09.020

Deshpande, O., de-Carvalho, J., Vieira, D. V. and Telley, I. A. (2021). Astral microtubule crosslinking by Feo safeguards uniform nuclear distribution in the Drosophila syncytium. *J. Cell Biol.* **221**, e202007209. doi:10.1083/jcb.202007209

Donoughe, S., Hoffmann, J., Nakamura, T., Rycroft, C. H. and Extavour, C. G. (2021). Local density determines nuclear movements during syncytial blastoderm formation in a cricket. *bioRxiv* 2021.04.26.441395.

Dutta, S., Djabrayan, N. J.-V., Torquato, S., Shvartsman, S. Y. and Krajnc, M. (2019). Self-similar dynamics of nuclear packing in the early Drosophila embryo. *Biophys. J.* **117**, 743-750. doi:10.1016/j.bpj.2019.07.009

Firestone, A. J., Weinger, J. S., Maldonado, M., Barlan, K., Langston, L. D., O'Donnell, M., Gelfand, V. I., Kapoor, T. M. and Chen, J. K. (2012). Small-molecule inhibitors of the AAA+ ATPase motor cytoplasmic dynein. *Nature* **484**, 125-129. doi:10.1038/nature10936

Foe, V. E. and Alberts, B. M. (1983). Studies of nuclear and cytoplasmic behaviour during the five mitotic cycles that precede gastrulation in Drosophila embryogenesis. *J. Cell Sci.* **61**, 31-70. doi:10.1242/jcs.61.1.31

Freeman, M. and Glover, D. M. (1987). The gnu mutation of Drosophila causes inappropriate DNA synthesis in unfertilized and fertilized eggs. *Gene Dev.* **1**, 924-930. doi:10.1101/gad.1.9.924

Freeman, M., Nüsslein-Volhard, C. and Glover, D. M. (1986). The dissociation of nuclear and centrosomal division in gnu, a mutation causing giant nuclei in Drosophila. *Cell* **46**, 457-468. doi:10.1016/0092-8674(86)90666-5

Garzon-Coral, C., Fantana, H. A. and Howard, J. (2016). A force-generating machinery maintains the spindle at the cell center during mitosis. *Sci New York N Y* **352**, 1124-1127. doi:10.1126/science.aad9745

Gönczy, P., Pichler, S., Kirkham, M. and Hyman, A. A. (1999). Cytoplasmic dynein is required for distinct aspects of mtoc positioning, including centrosome separation, in the one cell stage Caenorhabditis elegans embryo. *J. Cell Biol.* **147**, 135-150. doi:10.1083/jcb.147.1.135

Grill, S. W., Howard, J., Schäffer, E., Stelzer, E. H. K. and Hyman, A. A. (2003). The distribution of active force generators controls mitotic spindle position. *Science* **301**, 518-521. doi:10.1126/science.1086560

Hamaguchi, M. and Hiramoto, Y. (1980). Fertilization process in the heart-urchin, Clypeaster Japonicus observed with a differential interference microscope. *Dev. Growth Differ.* **22**, 517-530. doi:10.1111/j.1440-169X.1980.00517.x

Hatanaka, K. and Okada, M. (1991). Retarded nuclear migration in Drosophila embryos with aberrant F-actin reorganization caused by maternal mutations and by cytochalasin treatment. *Development* **111**, 909-920. doi:10.1242/dev.111.4.909

Hertwig, O. (1893). Ueber den Werth der ersten Furchungszellen für die Organbildung des Embryo Experimentelle Studien am Frosch-und Tritonei. *Archiv Für Mikroskopische Anatomie* **42**, 662-807. doi:10.1007/BF02976796

Holly, R. M., Mavor, L. M., Zuo, Z. and Blankenship, J. T. (2015). A rapid, membrane-dependent pathway directs furrow formation through RalA in the early Drosophila embryo. *Development* **142**, 2316-2328. doi:10.1242/dev.120998

Hughes, D. and Paczuski, M. (2001). Large scale structures, symmetry, and universality in sandpiles. *Phys. Rev. Lett.* **88**, 054302. doi:10.1103/PhysRevLett.88.054302

Hyman, A. A. (1989). Centrosome movement in the early divisions of Caenorhabditis elegans: a cortical site determining centrosome position. *J. Cell Biol.* **109**, 1185-1193. doi:10.1083/jcb.109.3.1185

Inoue, Y. H., Savoian, M. S., Suzuki, T., Máthé, E., Yamamoto, M.-T. and Glover, D. M. (2004). Mutations in orbit/mast reveal that the central spindle is comprised of two microtubule populations, those that initiate cleavage and those that propagate furrow ingression. *J. Cell Biol.* **166**, 49-60. doi:10.1083/jcb.200402052

Jo, W. S., Yi, S. D., Baek, S. K. and Kim, B. J. (2012). Cluster-size heterogeneity in the two-dimensional Ising model. *Phys. Rev. E* **86**, 032103. doi:10.1103/PhysRevE.86.032103

Kaiser, F., Lv, Z., Marques Rodrigues, D., Rosenbaum, J., Aspelmeier, T., Großhans, J. and Alim, K. (2018). Mechanical model of nuclei ordering in Drosophila embryos reveals dilution of stochastic forces. *Biophys. J.* **114**, 1730-1740. doi:10.1016/j.bpj.2018.02.018

Kanesaki, T., Edwards, C. M., Schwarz, U. S. and Grosshans, J. (2011). Dynamic ordering of nuclei in syncytial embryos: a quantitative analysis of the role of cytoskeletal networks. *Integr. Biol.* **3**, 1112-1119. doi:10.1039/c1ib00059d

Kimura, K. and Kimura, A. (2011). Intracellular organelles mediate cytoplasmic pulling force for centrosome centration in the Caenorhabditis elegans early embryo. *Proc. Natl. Acad. Sci. USA* **108**, 137-142. doi:10.1073/pnas.1013275108

Krzic, U., Gunther, S., Saunders, T. E., Streichan, S. J. and Hufnagel, L. (2012). Multiview light-sheet microscope for rapid in toto imaging. *Nat. Methods* **9**, 730-733. doi:10.1038/nmeth.2064

Lecuit, T. and Wieschaus, E. (2000). Polarized insertion of new membrane from a cytoplasmic reservoir during cleavage of the Drosophila embryo. *J. Cell Biol.* **150**, 849-860. doi:10.1083/jcb.150.4.849

Lee, L. A., Van Hoewyk, D. and Orr-Weaver, T. L. (2003). The Drosophila cell cycle kinase PAN GU forms an active complex with PLUTONIUM and GNU to regulate embryonic divisions. *Gene Dev.* **17**, 2979-2991. doi:10.1101/gad.1132603

Lv, Z., Rosenbaum, J., Aspelmeier, T. and Großhans, J. (2018). A 'molecular guillotine' reveals the interphase function of Kinesin-5. *J. Cell Sci.* **131**, jcs210583. doi:10.1242/jcs.210583

Lv, Z., Rosenbaum, J., Mohr, S., Zhang, X., Kong, D., Preiß, H., Kruss, S., Alim, K., Aspelmeier, T. and Großhans, J. (2020). The emergent yo-yo movement of nuclei driven by cytoskeletal remodeling in pseudo-synchronous mitotic cycles. *Curr. Biol.* **30**, 2564-2573.e5. doi:10.1016/j.cub.2020.04.078

Maliga, Z., Kapoor, T. M. and Mitchison, T. J. (2002). Evidence that monastrol is an allosteric inhibitor of the mitotic kinesin Eg5. *Chem. Biol.* **9**, 989-996. doi:10.1016/S1074-5521(02)00212-0

Meaders, J. L., de Matos, S. N. , and Burgess, D. R. (2020). A pushing mechanism for microtubule aster positioning in a large cell type. *Cell Rep.* **33**, 108213. doi:10.1016/j.celrep.2020.108213

Megraw, T. L., Li, K., Kao, L. R. and Kaufman, T. C. (1999). The centrosomin protein is required for centrosome assembly and function during cleavage in Drosophila. *Development* **126**, 2829-2839. doi:10.1242/dev.126.13.2829

Menzel, A. M. and Ohta, T. (2012). Soft deformable self-propelled particles. *Epl-europhys Lett.* **99**, 58001. doi:10.1209/0295-5075/99/58001

Minc, N., Burgess, D. and Chang, F. (2011). Influence of cell geometry on division-plane positioning. *Cell* **144**, 414-426. doi:10.1016/j.cell.2011.01.016

Mitchison, T., Wühr, M., Nguyen, P., Ishihara, K., Groen, A. and Field, C. M. (2012). Growth, interaction, and positioning of microtubule asters in extremely large vertebrate embryo cells. *Cytoskeleton* **69**, 738-750. doi:10.1002/cm.21050

Nestor-Bergmann, A., Goddard, G. and Woolner, S. (2014). Force and the spindle: mechanical cues in mitotic spindle orientation. *Semin. Cell Dev. Biol.* **34**, 133-139. doi:10.1016/j.semcdb.2014.07.008

Nguyen, P. A., Groen, A. C., Loose, M., Ishihara, K., Wühr, M., Field, C. M. and Mitchison, T. J. (2014). Spatial organization of cytokinesis signaling reconstituted in a cell-free system. *Science* **346**, 244-247. doi:10.1126/science.1256773

Paz, J. and Lüders, J. (2018). Microtubule-organizing centers: towards a minimal parts list. *Trends Cell Biol.* **28**, 176-187. doi:10.1016/j.tcb.2017.10.005
Perondini, A. L. P., Gutzeit, H. O. and Mori, L. (1986). Nuclear division and migration during early embryogenesis of *Bradysia tritici* coquillet (syn. *Sciara ocellaris*) (diptera: Sciaridae). *Int. J. Insect Morphol. Embryol.* **15**, 155-163. doi:10.1016/0020-7322(86)90054-1
Petkova, M. D., Tkačik, G., Bialek, W., Wieschaus, E. F. and Gregor, T. (2019). Optimal decoding of cellular identities in a genetic network. *Cell* **176**, 844-855.e15. doi:10.1016/j.cell.2019.01.007
Pflüger, E. (1884). Ueber die Einwirkung der Schwerkraft und anderer Bedingungen auf die Richtung der Zelltheilung. *Archiv Für Die Gesamte Physiologie Des Menschen Und Der Tiere* **34**, 607-616. doi:10.1007/BF01612880
Pierre, A., Sallé, J., Wühr, M. and Minc, N. (2016). Generic theoretical models to predict division patterns of cleaving embryos. *Dev. Cell* **39**, 667-682. doi:10.1016/j.devcel.2016.11.018
Postner, M. A., Miller, K. G. and Wieschaus, E. F. (1992). Maternal effect mutations of the sponge locus affect actin cytoskeletal rearrangements in Drosophila melanogaster embryos. *J. Cell Biol.* **119**, 1205-1218. doi:10.1083/jcb.119.5.1205
Raff, J. W. and Glover, D. M. (1989). Centrosomes, and not nuclei, initiate pole cell formation in Drosophila embryos. *Cell* **57**, 611-619. doi:10.1016/0092-8674(89)90130-X
Rappaport, R. (1961). Experiments concerning the cleavage stimulus in sand dollar eggs. *J. Exp. Zool.* **148**, 81-89. doi:10.1002/jez.1401480107
Rauzi, M., Lenne, P.-F. and Lecuit, T. (2010). Planar polarized actomyosin contractile flows control epithelial junction remodelling. *Nature* **468**, 1110-1114. doi:10.1038/nature09566
Robinson, J. T., Wojcik, E. J., Sanders, M. A., McGrail, M. and Hays, T. S. (1999). Cytoplasmic dynein is required for the nuclear attachment and migration of centrosomes during mitosis in Drosophila. *J. Cell Biol.* **146**, 597-608. doi:10.1083/jcb.146.3.597
Saw, T. B., Doostmohammadi, A., Nier, V., Kocgozlu, L., Thampi, S., Toyama, Y., Marcq, P., Lim, C. T., Yeomans, J. M. and Ladoux, B. (2017). Topological defects in epithelia govern cell death and extrusion. *Nature* **544**, 212-216. doi:10.1038/nature21718
Schindelin, J., Arganda-Carreras, I., Frise, E., Kaynig, V., Longair, M., Pietzsch, T., Preibisch, S., Rueden, C., Saalfeld, S., Schmid, B. et al. (2012). Fiji: an open-source platform for biological-image analysis. *Nat. Methods* **9**, 676-682. doi:10.1038/nmeth.2019
Schmidt, A. and Grosshans, J. (2018). Dynamics of cortical domains in early Drosophila development. *J. Cell Sci.* **131**, jcs212795. doi:10.1242/jcs.212795
Schubiger, G. and Edgar, B. (1994). Using inhibitors to study embryogenesis. *Methods Cell Biol.* **44**, 697-713. doi:10.1016/S0091-679X(08)60939-5
Shamanski, F. L. and Orr-Weaver, T. L. (1991). The Drosophila plutonium and pan gu genes regulate entry into S phase at fertilization. *Cell* **66**, 1289-1300. doi:10.1016/0092-8674(91)90050-9
Sharp, D. J., Yu, K. R., Sisson, J. C., Sullivan, W. and Scholey, J. M. (1999). Antagonistic microtubule-sliding motors position mitotic centrosomes in Drosophila early embryos. *Nat. Cell Biol.* **1**, 51-54. doi:10.1038/9025
Sommer, R. and Tautz, D. (1991). Asynchronous mitotic domains during blastoderm formation in Musca domestica L. (Diptera). *Roux's Arch. Dev. Biol.* **199**, 373-376. doi:10.1007/BF01705931
Sulerud, T., Sami, A. B., Li, G., Kloxin, A., Oakey, J. and Gatlin, J. (2020). Microtubule-dependent pushing forces contribute to long-distance aster movement and centration in Xenopus laevis egg extracts. *Mol. Biol. Cell* **31**, 2791-2802. doi:10.1091/mbc.E20-01-0088
Tanimoto, H., Kimura, A. and Minc, N. (2016). Shape–motion relationships of centering microtubule asters. *J. Cell Biol.* **212**, 777-787. doi:10.1083/jcb.201510064
Tanimoto, H., Sallé, J., Dodin, L. and Minc, N. (2018). Physical forces determining the persistency and centring precision of microtubule asters. *Nat. Phys.* **14**, 848-854. doi:10.1038/s41567-018-0154-4
Telley, I. A., Gáspár, I., Ephrussi, A. and Surrey, T. (2012). Aster migration determines the length scale of nuclear separation in the Drosophila syncytial embryo. *J. Cell Biol.* **197**, 887-895. doi:10.1083/jcb.201204019
Telley, I. A., Gáspár, I., Ephrussi, A. and Surrey, T. (2013). A single Drosophila embryo extract for the study of mitosis ex vivo. *Nat. Protoc.* **8**, 310-324. doi:10.1038/nprot.2013.003
Tinevez, J.-Y., Perry, N., Schindelin, J., Hoopes, G. M., Reynolds, G. D., Laplantine, E., Bednarek, S. Y., Shorte, S. L. and Eliceiri, K. W. (2017). TrackMate: an open and extensible platform for single-particle tracking. *Methods* **115**, 80-90. doi:10.1016/j.ymeth.2016.09.016
Vaizel-Ohayon, D. and Schejter, E. D. (1999). Mutations in centrosomin reveal requirements for centrosomal function during early Drosophila embryogenesis. *Curr. Biol.* **9**, 889-898. doi:10.1016/S0960-9822(99)80393-5
Valdés-pérez, R. E. and Minden, J. S. (1995). Drosophila melanogaster syncytial nuclear divisions are patterned: time-lapse images, hypothesis and computational evidence. *J. Theor. Biol.* **175**, 525-532. doi:10.1006/jtbi.1995.0160
von Dassow, G. and Schubiger, G. (1994). How an actin network might cause fountain streaming and nuclear migration in the syncytial Drosophila embryo. *J Cell Biology* **127**, 1637-1653. doi:10.1083/jcb.127.6.1637
von Dassow, G., Verbrugghe, K. J. C., Miller, A. L., Sider, J. R. and Bement, W. M. (2009). Action at a distance during cytokinesis. *J. Cell Biol.* **187**, 831-845. doi:10.1083/jcb.200907090
Wühr, M., Dumont, S., Groen, A. C., Needleman, D. J. and Mitchison, T. J. (2009). How does a millimeter-sized cell find its center? *Cell Cycle* **8**, 1115-1121. doi:10.4161/cc.8.8.8150
Wühr, M., Tan, E. S., Parker, S. K., Detrich, H. W. and Mitchison, T. J. (2010). A model for cleavage plane determination in early amphibian and fish embryos. *Curr. Biol.* **20**, 2040-2045. doi:10.1016/j.cub.2010.10.024
Zalokar, M. and Erk, I. (1976). Division and migration of nuclei during early embryogenesis of Drosophila melanogaster. *J. Microscopie Biol. Cell.* **25**, 97-106.